Linking optics and mechanics in an *in vivo* model of airway fibrosis and epithelial injury

Christopher B. Raub
University of California, Irvine
Department of Biomedical Engineering
Irvine, California 92697

Sari Mahon
University of California, Irvine
Beckman Laser Institute
Irvine, California 92697

Navneet Narula
University of California, Irvine
Department of Pathology
Irvine, California 92697

Bruce J. Tromberg
University of California, Irvine
Department of Biomedical Engineering
    and
Department of Surgery
    and
Beckman Laser Institute
Irvine, California 92697

Matthew Brenner
University of California, Irvine
Department of Medicine
Irvine, California 92697

Steven C. George
University of California, Irvine
Department of Biomedical Engineering
    and
Department of Chemical Engineering
    and Material Science
Irvine, California 92697

Abstract. Chronic mucosal and submucosal injury can lead to persistent inflammation and tissue remodeling. We hypothesized that microstructural and mechanical properties of the airway wall could be derived from multiphoton images. New Zealand White rabbits were intubated, and the tracheal epithelium gently denuded every other day for five days (three injuries). Three days following the last injury, the tracheas were excised for multiphoton imaging, mechanical compression testing, and histological analysis. Multiphoton imaging and histology confirm epithelial denudation, mucosal ulceration, subepithelial thickening, collagen deposition, immune cell infiltration, and a disrupted elastin network. Elastase removes the elastin network and relaxes the collagen network. Purified collagenase removes epithelium with subtle subepithelial changes. Young's modulus $[(E)$ measured in kiloPascal] was significantly elevated for the scrape injured (9.0 ± 3.2) trachea, and both collagenase (2.6 ± 0.4) and elastase (0.8 ± 0.3) treatment significantly reduced E relative to control (4.1 ± 0.7). E correlates strongly with second harmonic generation (SHG) signal depth decay for enzyme-treated and control tracheas $(R^2 = 0.77)$, but not with scrape-injured tracheas. We conclude that E of subepithelial connective tissue increases on repeated epithelial wounding, due in part to changes in elastin and collagen microstructure and concentration. SHG depth decay is sensitive to changes in extracellular matrix content and correlates with bulk Young's modulus. © *2010 Society of Photo-Optical Instrumentation Engineers.*
    [DOI: 10.1117/1.3322296]

Keywords: second harmonic; two photon fluorescence; collagen; elastin; fibrosis.

Paper 09262R received Jun. 23, 2009; revised manuscript received Nov. 20, 2009; accepted for publication Dec. 18, 2009; published online Feb. 22, 2010.

1 Introduction

Fibrosis and tissue remodeling often follows mucosal injury.[1–3] Various soluble factors from damaged epithelium and immune cells promote myofibroblast activation and subsequent fibrosis, including transforming growth factor (TGF)-β1 and -β2, interleukin (IL)-13, and platelet-derived growth factor (PDGF).[1–5] Mucosal stiffening resulting from increased collagen deposition and cross-linking can impact normal function at both cell and tissue levels and provide mechanical cues that promote further scar formation (e.g., matrix stiffness-dependent strain-induced TGF-β activation).[6,7] Although elastography is a promising technique

that maps tissue strain, it typically possesses limited spatial resolution and biochemical discrimination;[8] hence, there remain limited methods to noninvasively assess tissue remodeling and the mechanical properties of mucosal tissue.

Mucosal injury can include epithelial denudation and cell shedding, resulting in ulceration followed by cell migration and proliferation to rapidly reepithelialize the mucosa. In the subepithelial tissue, there may be immediate hemorrhage and fibrin clot formation, followed rapidly by edema and neutrophil invasion, resolving after one to three weeks to persistent macrophage presence, fibroplasia, and fibrosis.[9] An improved understanding of changes in matrix mechanics and biochemical signals in the first week following injury may facilitate the treatment of fibrotic diseases of mucosa, such as asthma and interstitial lung diseases. Recently, *in vitro* and *in vivo* models

Address all correspondence to: Steven C. George, M.D., Ph.D., Department of Biomedical Engineering, 2420 Engineering Hall, University of California, Irvine, Irvine, California 92697-2730. Tel.: (949) 824-3941; Fax: (949) 824-9968; E-mail: scgeorge@uci.edu

of airway epithelial scrape wounding have received attention as relevant models of mucosal injury, wound healing, and tissue remodeling.[10–12]

Previously, we have shown that multiphoton microscopy (MPM), used to image second harmonic generation (SHG) from collagen gels, can accurately assess matrix microstructure and predict bulk tissue stiffness.[13,14] SHG arises uniquely from noncentrosymmetric molecular arrays possessing a nonlinear susceptibility, such as collagen fibrils. In contrast, two-photon fluorescence (TPF) arises from endogenous fluorophores such as NAD(P)H and FAD+ in cells,[15–17] or pyridinium-type cross-links in matrix molecules.[18,19] More recent reports on the feasibility of multiphoton endoscopy have demonstrated the potential to utilize both SHG and TPF signals *in vivo*.[20–22] Thus, MPM imaging of SHG and TPF signals from normal and scrape-wounded tracheal mucosa may noninvasively characterize changes to epithelium, leukocytes, collagen, and elastin that lead to fibrotic tissue remodeling and stiffening.

Correlating such cellular and microstructural information with tissue stiffness (measured by indentation testing) could provide novel information linking inflammation, fibrosis, and stiffness-dependent wound healing. We developed a repeated airway epithelial injury model, in which the tracheal mucosa of a rabbit is injured every other day for five days (three scrapes) and then excised three days after the last injury. Following excision, we performed MPM imaging, indentation testing, and histological analysis of the mucosa, comparing the wounded tissue to normal tissue, as well as to elastase and collagenase-treated tracheal sections. Young's modulus in compression (E) was then correlated with MPM imaging parameters to explain the effects of changes in collagen, elastin, epithelium, and immune cells on bulk tissue mechanics.

2 Materials and Methods

2.1 Animal Procedures

All procedures involving animals were approved by the Institutional Animal Care and Use Committee. All animals were treated in accordance with federal and state regulatory guidelines. Seventeen New Zealand White rabbits (nine controls and eight scrape-injured) weighing 3–5 kg (Western Oregon Rabbit Company, Philomath, Oregon) were anesthetized, intubated [see Fig. 1(a)], and maintained under anesthesia as previously described[23] with the following differences: 0.2 mL maintenance anesthetic was administered by injection every 5 min, rather than continuously. The tracheal scrape procedure was performed as previously described.[11] Briefly, rabbits were scraped on three occasions—every other day for five days—and were then sacrificed three days after the final scrape. Some animals were sacrificed immediately after the first scrape in order to distinguish between immediate and long-term effects of the injuries. A 7-mm-diam unsheathed cytology brush [Conmed, Utica, New York; see Fig. 1(b)] was inserted through the endotracheal tube and scraped over the entire length of exposed tracheal lumen between the endotracheal tube opening and the carina (~3 cm). The brush was scraped against the tracheal mucosa for ~15 s. Cells on the brush were shaken into 1 mL of phosphate buffered saline (PBS) containing 4% formaldehyde and were subsequently stained with Alexafluor 568 phalloidin (Invitrogen, Carlsbad,
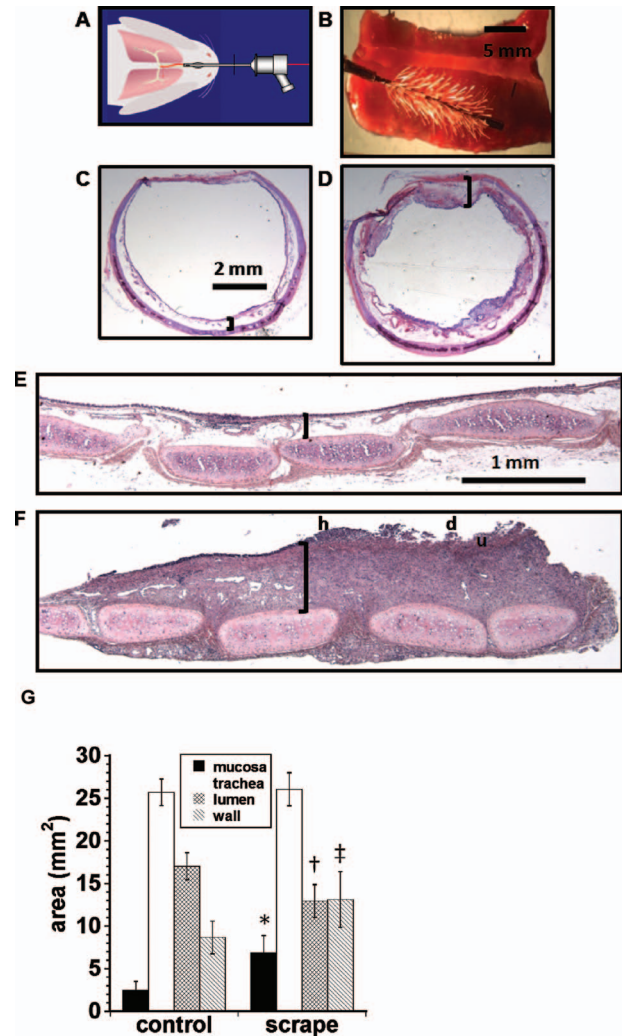

Fig. 1 Experimental schematic and low-magnification images of unwounded and scrape-wounded tracheas. (a) Diagram showing endotracheal intubation of an anesthetized rabbit that allowed nonsurgical access to the distal 3 cm of the tracheal mucosa and submucosa for scrape wounding. (b) Dissecting microscope view of an excised portion of a scraped trachea, cut along the trachealis to expose the lumen, plus the cytology brush used to create the scrape wound. H&E stained 5-μm-thick circumferential sections of (c) control and (d) scrape-wounded tracheas. H&E stained 5-μm sagittal sections (transverse to cartilage rings) of (e) control and (f) scrape-wounded tracheas. Mucosal thickness is indicated by solid black brackets. d, u, and h represent areas of denuded, ulcerated, and hyperplastic epithelium, respectively. (g) Quantification from circumferential histological sections of morphological changes after chronic scrape wounding. Scrape-wounded mucosa and wall cross-sectional area are significantly greater than control areas (t-test, *p* value <0.001 and *p* value <0.01, respectively). Lumen cross-sectional area is significantly decreased (*t* test, *p* value <0.001). ∗, †, and ‡ indicate statistical significance relative to corresponding control. Control N=3 rabbits; scrape N=6 rabbits.

California) and DAPI (Sigma, St. Louis, Missouri). Phase contrast and epifluorescence microscopy confirmed the presence of clusters of columnar ciliated epithelial cells (data not shown), as well as erythrocytes in the brushings. Rigid bronchoscopy confirmed placement of the endotracheal tube and gross appearance of the tracheal lumen, which appeared ul-

cerated and edematous following the second and third scrape injuries. Optical coherence tomography (OCT) was also performed on the tracheal mucosa as previously described,[23] confirming development of mucosal edema 10 min following the brush injury. Following the scrape injuries and recovery periods (or similar time period for control animals), the rabbits were euthanized as described previously.[23]

2.2 Multiphoton Imaging

Rabbit tracheas were excised following euthanasia and stored in 50 mL of ice-cold PBS until removal for imaging ($\sim 2-3$ h). In addition, six control tracheas from nonintubated, noninjured rabbits were cut into strips encompassing one-third of the tracheal circumference and subjected to 1 mg/mL CLSPA collagenase (Worthington, Biochemical Corporation, Lakewood, New Jersey) in PBS; 4.5 mg/mL ESL elastase in 0.2 M Tris-HCl buffer, pH 8.8; or no enzyme for a period of 24 h. Imaging and mechanical testing of these enzyme-treated and control tracheas commenced after several rinses in fresh PBS, and MPM images of these control tracheas were found to be indistinguishable from tracheas imaged at earlier time points. All tracheas were cut along the trachealis [for example, see Fig. 1(b)] and then into $\sim 4 \times 4$ mm rectangular sections. Tracheal sections were sandwiched between two circular no. 1 borosilicate coverglasses (Fisher, Hampton, New Hampshire) and maintained in a hydrated state during imaging. All imaging was performed on a Zeiss 510 Meta multiphoton laser scanning microscope (Zeiss, Jena, Germany). SHG and TPF signals were collected in the epiconfiguration with an Achroplan $40\times/0.8$ NA water-immersion objective, and 12-bit images contained 512×512 pixels, with pixel size 0.44 μm. A circularly polarized Chameleon laser (Coherent Incorporated, Santa Clara, California) was focused on the trachea samples at wavelength 920 nm with incident power $\sim 60-175$ mW (laser power was increased for more highly scattering samples). SHG signal was collected using a $390-465$ nm infrared-blocking bandpass filter; TPF signal was collected simultaneously in a different channel using a $500-500$ nm infrared-blocking bandpass filter. Two scans were averaged per frame with a pixel dwell time of 1.60 μs. Three to ten serial depth sections with $2-10$ μm vertical spacing between individual frames ("z stacks") were recorded per trachea section, with at least 225 μm between stacks. Additionally, 25 individual frames were tiled together laterally to form one large 1.125 $\times 1.125$ mm tiled image for control and scrape-injured trachea sections.

2.3 Mechanical Testing

Indentation testing was performed using a 1.3-mm-diam cylindrical platen to indent samples at a rate of 0.05 mm/s up to 0.1 mm. After multiphoton imaging, the trachea sections were placed in PBS and transported to a Synergie 100 testing system (MTS Systems Corporation, Eden Prairie, Minnesota). Samples were placed on 600-grade ultrafine waterproof sandpaper (3M, St. Paul, Minnesota) during the test. A 1.3-mm-diam platen was placed just touching the tracheal mucosa, and stress and strain were recorded for a 100-μm

indentation. The Young's modulus in compression (E) was calculated as the best-fit slope of the resulting stress-strain curve.

2.4 Histological Procedures

Standard procedures were used to prepare histological stains of tracheal sections. Tracheas were paraffin embedded and sectioned in 5-μm-thin sections. Sections were prepared parallel and perpendicular to the long axis of the trachea. Masson's trichrome, Verhoeff-van Gieson (VVG), and hematoxylin and eosin (H&E) stains were performed on serial tissue sections in order to analyze collagen, elastin, and cell content of the tissues. Additionally, some tracheas were flash frozen in OCT medium (Ted Pella Incorporated, Redding, California), and then sectioned on a cryotome to 20-μm sections. These sections were sufficiently thick to image with MPM after thawing in PBS. Following MPM imaging, these sections were stained in a fashion similar to the 5-μm histology sections.

2.5 Image Analyses

All image analysis was performed with ImageJ (Wayne Rasband, NIH, Bethesda, Maryland), and $10\times$ magnified brightfield images of histologically stained circumferential sections were manually thresholded to distinguish tissue from the background. Various tissue and layer edges were traced in order to determine average areas of the tracheal lumen, the tracheal wall, the entire wall plus lumen, and the mucosa only (i.e., tissue inward of the tracheal rings). Five control and six scrape-injured trachea sections from separate rabbits were analyzed in this way.

$200\times$ magnified bright-field images of Masson's trichrome and VVG-stained trachea sections were analyzed to estimate image area occupied by collagen and elastin, respectively. RGB images of Masson's trichrome images were split, and the blue channel, solely, was analyzed. The blue image, containing blue-stained collagen, was manually thresholded, and the entire mucosa from cartilage to lumen was traced. The fraction of blue-stained pixels was then determined. Raw RGB images of VVG-stained sections were inverted and thresholded in order to separate the elastin (originally stained black) from tissue stained with a lighter shade. Regions of tissue containing elastin were then traced, and the percent of elastin-containing pixels was measured.

Four parameters were quantified from SHG and TPF images of the tracheas: SHG and TPF signal area fractions, and the segmented and raw SHG signal intensity depth decay coefficients. Single images from z stacks containing the brightest SHG and TPF signal, respectively, were collected from each trachea sample and pooled for analysis. Each image was manually thresholded to determine the cutoff between noise and void-containing pixels and signal-containing pixels, and the area fraction of signal was determined. SHG signal intensity decay coefficients were calculated from an exponential best fit of z-stack image intensities plotted against depth from the luminal surface. All images were noise subtracted (determined from the image intensity of a z-stack frame positioned below the tissue surface). Images were further thresholded as before to isolate signal-containing pixels, and the segmented mean of these signal-containing pixels were also plotted as a

decaying function of tissue depth. The SHG decay coefficient is defined as b in the following best-fit equation: SHG intensity $= Ae^{-bz}$ where z is depth from the tissue surface in millimeters and A and b are constants determined by the best fit.

2.6 Statistical Analysis

Student's t-test was used to distinguish significant differences between measurements from control and scrape-injured histology sections. Mean E of control, scrape-injured, collagenase-treated, and elastase-treated tracheas were compared to a single analysis of variance (ANOVA) test, followed by a *post hoc* Tukey test. A p value of 0.05 or less was considered significant. Correlations of E with TPF area fraction, SHG area fraction, raw SHG decay, and segmented SHG decay were performed with linear best fits, and R^2 values were determined. All error bars represent standard deviation, unless otherwise stated.

3 Results

3.1 Histological Comparison of Uninjured and Scrape-Injured Tracheas

Injured tracheas developed whitish granulation tissue and increased mucus, easily removed by gentle rinsing postsacrifice, compared to controls. H&E stained circumferential sections [Fig. 1(d)] and sagittal sections [Fig. 1(f)] of injured tracheas display marked fibrosis and mucosal thickening [Figs. 1(d) and 1(f), brackets] with regions of denuded epithelium [Fig. 1(f), labeled d] and ulcerated tissue [Fig. 1(f), labeled u] neighboring hyperplastic epithelium [Fig. 1(f), labeled h]. The airway luminal area is decreased, and the mucosal border is irregular [Fig. 1(d)]. In comparison, circumferential and sagittal sections of uninjured tracheas [Figs. 1(c) and 1(e) respectively] display thin subepithelial connective tissue [Fig. 1(c) and 1(e), brackets]. Higher magnification images of VVG-stained sections of uninjured tracheas show unbroken and normal differentiated epithelium [best seen in Fig. 2(b), e]. Quantified from circumferential sections, mucosal area increased $\sim$150% (6.9 ± 2.0 mm^2 versus 2.5 ± 1.0 mm^2 for injured and control, respectively, p value <0.001); area of the tracheal wall increased $\sim$50% (13.1 ± 3.3 mm^2 versus 8.7 ± 1.9 mm^2 for injured and control, respectively, see p value <0.01); and lumen cross-sectional area decreased $\sim$25% (13.0 ± 1.9 mm^2 versus 17.0 ± 1.6 mm^2 for injured and control, respectively, p value <0.001); while total area of the cross sections were similar (26.1 ± 2.0 mm^2 versus 25.7 ± 1.5 mm^2 for injured and control, respectively, no significant difference, p value $=0.68$).

Damaged blood vessels, fibrin, and primarily lymphocytic infiltration are visible at high magnification [Fig 2(d)]. Scrape-injured sections contained more than a three-fold increase in immune cells—mostly polymorphonuclear neutrophils [Fig. 2(d) inset, labeled n], and lymphocytes characterized by round heterochromatic nuclei [Fig. 2(d) inset, labeled L; 47 ± 9 and 162 ± 52 cells/400$\times$ field of view for control and scrape-injured tracheas, respectively, two-tailed t-test, p value <0.001]. Masson's trichrome and VVG stains of serial sections revealed the nature of mucosal collagen and elastin [Figs. 2(a)–2(d)]. In uninjured tracheas the lamina reticularis
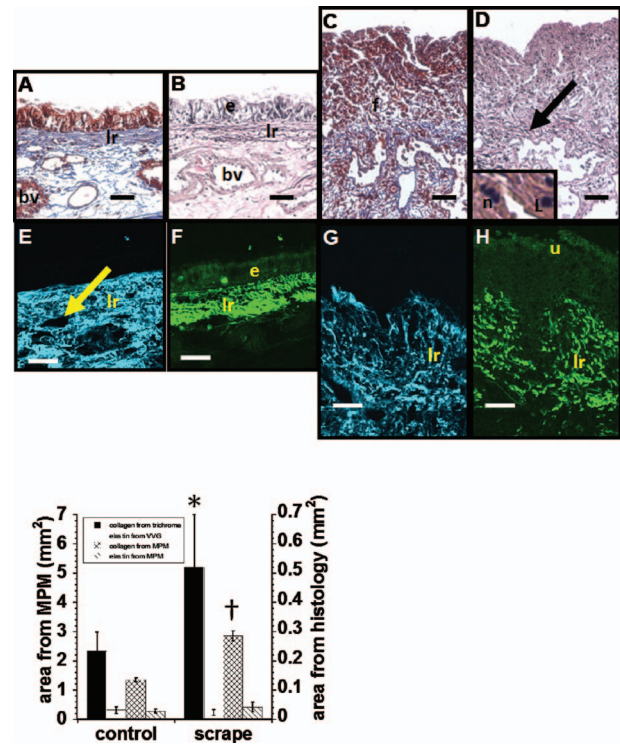

Fig. 2 Comparison of histology and MPM images of trachea sections. Masson's trichrome stain and Verhoeff-van Gieson (VVG) stain of control trachea (a, b, respectively) and scrape-wounded trachea (e, F, respectively) 5-μm-thick sections. Coregistered SHG and TPF images of control trachea (c, d, respectively) and scrape-wounded trachea (g, h, respectively) from 20 μm cryosections. bv, lr, e, f, n, L, and u represent blood vessel, lamina reticularis, epithelium, fibrosis, neutrophil, lymphocyte, and ulcerated epithelium, respectively. Black and yellow arrows represent damage to the elastic fiber network in the lamina reticularis and a blood vessel, respectively. (i) Quantification of area covered by collagen (assessed from trichrome stain and cryosection SHG) and by elastic fibers (assessed from VVG stain and cryosection TPF). Collagen cross-sectional area is significantly increased in the scrape-wounded tracheas (t-test, p value <0.0001 and p value <0.01, from trichrome and SHG images, respectively). $*$ and $\dagger$ indicate statistical significance relative to corresponding control). Control $N=3$ cryosections from three rabbits; nine histological sections from three rabbits; scrape $N=5$ cryosections from five rabbits; and 12 histological sections from four rabbits. Scale bars are 50 μm.

(labeled lr) forms a thin (30–80 μm) layer of dense, interwoven collagen [Fig. 2(a)] and elastic fiber [Fig. 2(b)] networks. Beneath the lamina reticularis, sparse subepithelial collagen surrounds small blood vessels [Figs. 2(a) and 2(b) labeled bv]. In injured tracheas the organization of the lamina reticularis is lost, with extensive fibrotic collagen (labeled f) deposited apically near the site of injury [Fig. 2(c)] concurrent with distortion of the collagen network and damage to the elastic fiber network in the lamina reticularis [Fig. 2(d), damage indicated by arrow].

Multiphoton images of 20-μm-thick frozen [Figs. 2(e)–2(h)] sections revealed similar information as histology sections, but the uniqueness, in these conditions, of SHG signal to collagen and TPF signal to elastin and cells allows for clear discrimination of those tissue constituents. The origins of SHG signal from collagen and TPF signal from elastin, immune cells, epithelium, and fibrin exudates are confirmed

by comparison of MPM images of cryosections with Masson's trichrome and VVG-stained tracheal sections taken from serial sections of the same tracheal tissue. The lamina reticularis of uninjured tracheal sections contains a uniform and dense network of SHG-producing collagen [Fig. 2(e)] and TPF-producing elastin [Fig. 2(f)] basal to a uniform, columnar epithelium (e) which also emits a TPF signal [Fig. 2(f)]. Blood vessels are visible basal to and within the lamina reticularis as void space with little SHG signal [Fig. 2(e), yellow arrow]. Phalloidin-conjugated fluorophore staining of tracheal sections demonstrate the presence of blood vessels within these regions devoid of SHG and TPF signal [Fig. 2(c)]. In contrast, the scrape-wounded tracheal mucosa shows a thicker, less connected collagen and elastin network within a disrupted, nonuniform lamina reticularis, evidenced by SHG [Fig. 2(g)] and TPF [Fig. 2(h)] signal from these layers. The thickened epithelium is weakly autofluorescent, and a fibrin exudate/ulcer covers the jagged apical surface of the lamina reticularis [Fig. 2(h), labeled u]. From MPM images of the same trachea cryosections that span the whole tracheal cross section, the thickness of the uninjured epithelium is $35-60$ μm; the lamina reticularis is $45-90$ μm; and the whole tracheal wall is ~0.9 mm. In contrast, MPM images of the scrape-injured trachea cryosection reveal a fibrin layer thickness of $90-150$ μm, a lamina reticularis of $100-250$ μm, and a tracheal wall thickness of $1-1.5$ mm.

SHG images of scraped tracheas show a approximate two-fold greater area of mucosal collagen [Fig. 2(g) versus 2(e), p value <0.01), while the area of elastic fibers assessed from the TPF image does not significantly change (p value=0.24), though scrape injury clearly disrupts the elastic fiber network (see Figs. 3 and 4). A loss of epithelial-derived TPF signal was observed [Fig. 2(h) versus 2(f)], corresponding to ulcerated tissue replacing the denuded epithelium and visible in the histology sections [Figs. 2(c) and 2(d) versus 2(a) and 2(b)]. Figure 2(i) shows that changes to collagen and elastic fiber cross-sectional area determined from tracheal sections imaged with MPM or stained for histology display similar trends of increased collagen area within the mucosal tissue, with relatively unchanged cross-sectional areas of elastic fibers.

3.2 Microstructure Assessed by MPM

Taking advantage of the inherent depth-resolved nature of SHG and TPF signals, we were able to resolve the microstructural details of the uninjured and scrape-injured subepithelial matrices by imaging a plane of tiled images beneath the epithelium and fibrin clot, respectively, in whole, unfixed tracheas (Fig. 3). Beneath the uninjured epithelium lies an interspersed network of SHG-producing collagen fibers and TPF-producing elastic fibers [Fig. 3(a)]. The collagen fibers are thicker (2.3 ± 1.2 μm versus 1.7 ± 0.7 μm, p value <0.05, two-tailed t-test, $n=29$ collagen, and elastic fibers) and more sinuous, and both fibers are oriented preferentially in one direction (parallel to the tracheal cylindrical axis). The combined networks occupy most of the image area relatively homogeneously except for gaps that stain positive for f-actin [Fig. 3(c); red channel, labeled bv], and which histology reveals to be small blood vessels [Fig. 2(a), labeled bv].

In contrast, the scrape-injured trachea reveals an inhomogeneous network of finer collagen fibers (many not clearly
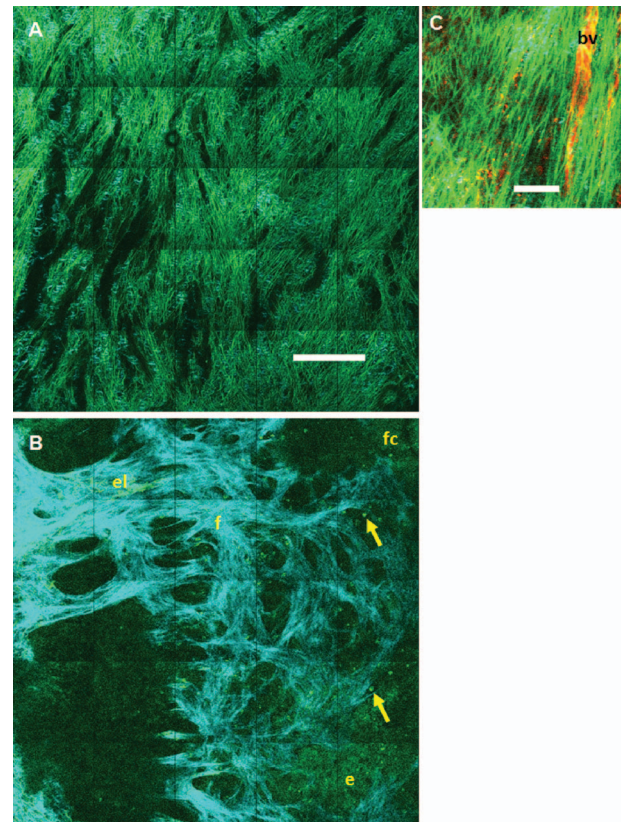

Fig. 3 *En face* MPM images of (a) control and (b) scrape-wounded tracheal submucosa showing SHG signal (blue) from collagen, and TPF signal (green) from elastin, immune cells, and epithelium. (c) *En face* MPM image of the lamina propria from a control trachea, displaying endogenous SHG (blue) and TPF (green) signals, as well as Alexafluor 568-conjugated phalloidin staining (red), revealing blood vessels and actin-rich cells. bv, fc, el, f, and e represent blood vessel, fibrin clot, elastin, collagen fiber, and epithelium, respectively. Arrows point to TPF signal consistent with immune cells. Images are ~30 μm below the surface and tiled together to display regional heterogeneity in the submucosa. The scale bars are 200 μm (a, b) and 50 μm (c).

resolvable as individual structures) deposited in a dense meshwork with random orientation [Fig. 3(b), labeled f]. Strongly fluorescing immune cells [Fig. 3(b), yellow arrows] are interspersed in a faintly autofluorescent fibrin clot [Fig. 3(b), labeled fc], with rare occurrence of areas of damaged elastin [Fig. 3(b), labeled el] and epithelium [Fig. 3(b), labeled e].

MPM z stacks of unmounted and unsectioned tracheal tissue show microstructures of uninjured rabbit tracheas and tracheas subjected to single scrape injury, triple scrape injury with recovery, elastase treatment, and collagenase treatment (Fig. 4). MPM images of uninjured tracheas display the previously described subepithelial collagen network [Figs. 4(a) *en face* and 4(c) axial view, blue signal, basal layer] and elastic fiber network [Figs. 4(b) *en face* and 4(c) axial view, green signal, basal layer] consistent with the lamina reticularis. MPM images of control tracheas also display normal epithelium [Fig. 4(c) axial view, green signal, apical layer] and lamina reticularis both $30-45$ μm thick [Fig. 4(c)]. A single scrape injury leaves the collagen network relatively intact [Fig. 4(d)], but breaks many elastic fibers [Fig. 4(e), damage indicated with yellow arrow] and denudes the epithelium [Fig.
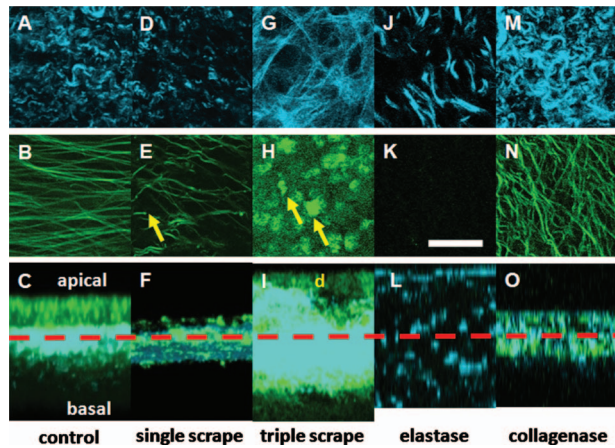
Fig. 4 MPM images characterize normal and altered submucosal extracellular matrix. Coregistered *en face* SHG and TPF images of tracheal submucosa (taken at the plane of the dotted red line) reveal changes in the SHG producing elements [i.e., collagen (a–e)] and TPF producing elements (f–j) of the superficial submucosa, consistent with elastin and immune cells. Z-stack projections of merged SHG and TPF images (k–o) reveal epithelial and subepithelial morphological changes in the apical-basal plane of the trachea. MPM images are from a control trachea (a, f, k), a single scrape-wounded trachea (b, g, l), a triple scrape-wounded trachea allowed to heal for three days (c, h, m), an elastase-treated trachea (d, i, n), and a collagenase-treated trachea (e, j, o). The dashed red line represents the approximate location of the corresponding *en face* images in (a)–(n). d represents damaged epithelium. The scale bar is 50 μm.

4(f)]. Tracheas subjected to three successive scrapes and allowed to heal for three days formed a dense meshwork of fibrotic collagen [Fig. 4(g)] interspersed with immune cells [Fig. 4(h), indicated by yellow arrows], and a partially restored, but damaged, epithelium mixed with fibrin clot apical to a thicker mucosal collagen layer [Fig. 4(i), labeled d]. These features are similar to the those seen in MPM images of tracheal sections [Figs. 2(e)–2(h)] and are confirmed by histology of tracheal sections [Fig. 2(a)–2(d)]. Elastase treatment allowed the collagen fibers to become more dispersed and relax from the sinuous, aligned network [Fig. 4(j)] as the surrounding elastic fiber network is almost completely degraded, as assessed by lack of TPF signal from these samples [Fig. 4(k)]. The collagen fiber layer expands and becomes sparser [Fig. 4(l)]. Collagenase removes the epithelium [Fig. 4(o)] but has little effect on the subepithelial collagen as assessed by SHG signal [Fig. 4(m)], although individual elastic fibers display increased curvature suggestive of possible stress relaxation [Fig. 4(n)].

3.3 Relationship of E with MPM Image Parameters

Figure 5 presents the mean and standard deviation of E, the Young's modulus in compression of the *ex vivo* tracheas. The mucosa of the scrape-injured tracheas allowed to heal for three days were the stiffest ($E=9.0\pm3.2$ kPa), followed by the uninjured tracheas ($E=4.1\pm0.7$ kPa). Collagenase-treated tracheas were somewhat less stiff than the control ($E=2.6\pm0.4$ kPa), and elastase-treated tracheas were the least stiff [$E=0.8\pm0.3$ kPa, Fig. 5(a)]. TPF and SHG signal area fractions largely failed to correlate with E [Figs. 5(b) and 5(c), respectively], except the modest and negative correlation
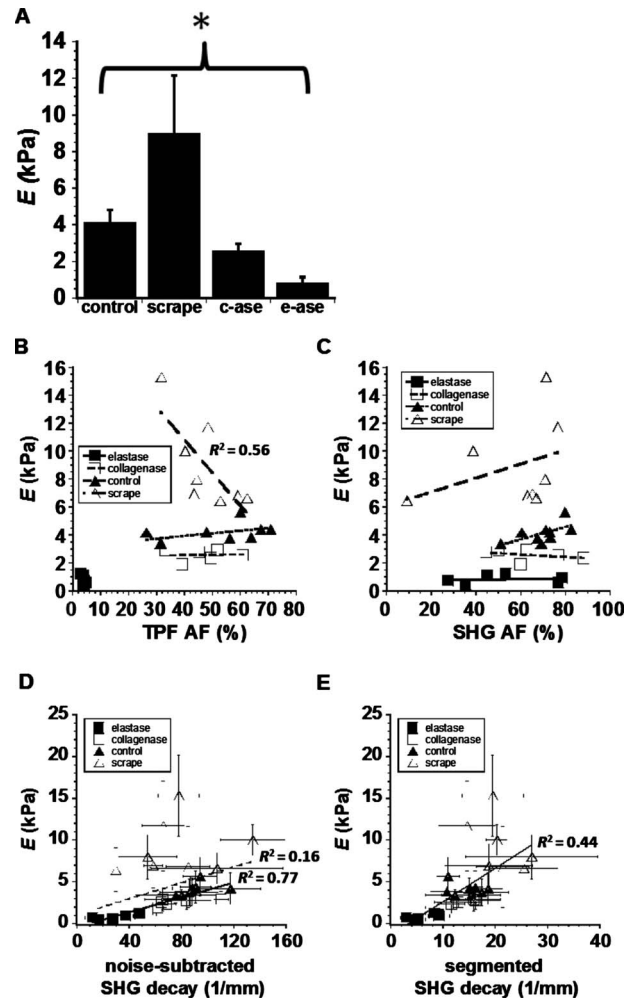

Fig. 5 Mechanical testing of tracheas: (a) Young's modulus in compression (E), measured in the low strain region by indentation testing to a depth of 100 μm on trachea sections varies significantly with experimental treatment of the tracheas. (ANOVA, p value <0.0001, * indicates statistical significance. $N=9$, 8, 6, and 6 tracheas for the control, chronic scrape, collagenase, and elastase-treated groups, respectively, with $n=6-14$ indentation tests performed per trachea over the distal, injured region). (b) E versus TPF signal area fraction from a representative z slice of the submucosa plotted for the control and three treatments. (c) E versus SHG signal area fraction from a representative z slice of the submucosa plotted for the control and three treatments. (d) E versus noise-subtracted SHG decay from MPM z stacks of the tracheal submucosa plotted for the control and three treatments. (e) E versus noise-subtracted SHG decay from MPM z stacks of the tracheal submucosa, segmented to examine only signal-containing pixels, plotted for the control and three treatments. $N=8$, 7, 6, and 6 tracheas for the control, chronic scrape, collagenase, and elastase-treated groups, respectively, with $n=3-10$ MPM z stacks imaged per trachea over varying locations on the distal portion. Linear best-fit lines to the data are shown with solid or dashed lines.

of E and TPF signal area fraction from scrape-injured mucosa [$R^2=0.56$; Fig. 5(b)]. E correlates highly with the SHG signal intensity decay coefficient from noise-subtracted images for the enzyme-treated and control tracheas only [$R^2=0.77$ versus $R^2=0.16$ from scrape-injured mucosa, Fig. 5(d)]. In contrast, E correlates modestly with the SHG signal intensity depth decay coefficient from segmented SHG images (excluding

void pixels in the calculation), including the scrape-injured tissues [$R^2 = 0.44$, Fig. 5(e)].

4 Discussion

Mucosal mechanics play an important role in the normal function of many tissues and organs. Tissue remodeling leading to increased stiffness may impact function, as in airways fibrosis,[24–26] keloids,[27] or surgical hypertrophic scarring.[28] Mucosal stiffening may also indirectly promote disease processes by increasing growth-factor release from the extracellular matrix.[6] Furthermore, changes to mucosal extracellular matrix are particularly relevant to epithelial-mesenchymal transition, an epithelial phenotype switch important during development, renal and lung fibrosis,[29,30] and cancer metastasis.[31] In this work, we find an early and significant fibrosis (with collagen deposition and elastin network damage) and mucosal stiffening (approximately twofold change in E from 4.1 to 9.0 kPa) in response to three epithelial scrape injuries over the course of five days. In contrast, collagenase and elastase degrade components of the subepithelial extracellular matrix, leading to a corresponding decrease in mucosal stiffness [2.6 and 0.8 kPa, respectively; Fig. 5(a)]. Strikingly, microstructural and cellular changes to the mucosa as a result of scrape-injury or enzyme treatment are revealed by MPM of intrinsic SHG from collagen and TPF from elastic fibers, epithelium, and immune cells (Figs. 3 and 4). However, the mucosal mechanical environment is complex, and variation in bulk E cannot be explained by variation in simple indices, such as SHG or TPF signal image area fraction [Figs. 5(b) and 5(c)]. We find a modest correlation between E and SHG signal intensity depth decay coefficient from segmented images ($R^2 = 0.44$). In contrast, E and the SHG depth decay coefficient from unsegmented images correlate strongly for control and enzyme-treated tracheas ($R^2 = 0.77$) but fail to correlate in scrape-injured tracheas.

A previous study of tracheal scrape injury demonstrated an early (day 1) response of the trachea to scrape wounding that included epithelial ulceration, deposition of fibrin, and edema in the lamina propria,[9] features that are also present three days following the current study's triple scrape procedure. Reepithelialization has been shown to occur within five days of the initial scrape wound, with fibrosis occurring from days 7 to 21.[9] Early responses (<day 9) to tracheal scrape wounding corroborated by other studies include infiltration of neutrophils, submucosal hypertrophy, and thickened collagen fibers.[12] The scrape-wounded tracheas in our current study therefore are in an early stage of wound healing, in which edema is prevalent and collagen deposition and fibrosis have been initiated. It is important to note that SHG signals depend on the square of collagen concentration and that TPF signals arising from cells, elastin, and fibrin exudate depend linearly on fluorophore concentration within these components. In addition, SHG and TPF parameters from images also are affected by extracellular matrix structure and bulk tissue scattering and absorption. Therefore, one would not predict a simple correlation between collagen or elastin concentration and MPM image parameters in the tracheal mucosa.

Image area fraction and depth-dependent decay of multiphoton signals have been used to assess relative changes to tissue architecture and content.[4,13,14,32–34] Exponential decay

models have been used to describe the depth dependence in turbid tissues of fluorescence,[35,36] second harmonic,[36] confocal reflectance,[37] and optical coherence[38] signals. Recently, confocal reflectance signal depth decay at a 488-nm wavelength was used to distinguish between mouse skin containing normal and mutant collagen possessing a finer microstructure. SHG signal is more specific (e.g., to collagen) and can be used to image deeper tissue than a reflectance signal due to the near-infrared fundamental frequency used to create SHG. Furthermore, previous studies have shown positive correlations between SHG parameters and collagen concentration in acellular collagen gels,[13] tumors,[39] and lung parenchyma.[33] Significantly, data in collagen gels show that gels with similar collagen concentration but varied microstructure possess different SHG signal area fraction and mechanical properties.[13]

The correlation of E and the SHG decay coefficients appear to be robust to elastase and collagenase treatment. These treatments have been shown previously to increase airway mucosal compliance,[40] while simple removal of the epithelium leaves the mucosal stiffness unchanged.[24] Bovine tracheal mucosa contains roughly 5% and 40% collagen and elastin, respectively, by dry weight.[41] The current study supports previous findings that collagen and elastin predominantly determine tracheal mucosal mechanics. SHG signal depth decay is affected directly by collagen concentration and microstructure and indirectly by elastic fiber scattering of SHG signal and is thus sensitive to several factors that influence mucosal stiffness. This sensitivity explains the robust correlation of E with SHG depth decay in the tracheal mucosa. In contrast, E correlates only weakly with the area fractions of SHG signal and TPF signal [Figs. 5(b) and 5(c)], suggesting that these image parameters alone do not yield sufficient information to determine mechanical properties in the tracheal mucosa.

Elastase-treated tissues had drastically reduced TPF signal area fractions due to loss of elastic fibers. The significant reduction in E following elastase treatment could either be a direct effect of losing elastin fibers or an indirect effect of collagen network relaxation [Fig. 4(j)]. In contrast, scrape-wounded and collagenase-treated tracheas had similar TPF and SHG signal image area fractions as control tracheas, despite histological and optical evidence of changes to collagen, elastin, and epithelium. The effects of collagenase were primarily seen in the loss of epithelium and relaxation of the elastin network [see Figs. 4(m)–4(o)]. The strong correlation of E with SHG signal depth decay from collagenase-treated mucosa suggests that the SHG depth decay coefficient is sensitive to structural changes in the tracheal mucosa caused by collagenase, which reduce mucosal stiffness.

In contrast, scrape wounding resulted in drastically altered collagen microstructure and replacement of the elastin signal with signal from fibrin and immune cells [see Figs. 4(g)–4(i)], and, not surprisingly, altered mucosal mechanics. Interestingly, scrape-injured mucosal E correlates negatively with TPF signal area fraction [$R^2 = 0.56$, Fig. 5(b)] and positively, although weakly, with SHG signal area fraction [Fig. 5(c)]. In these tissues, immune cells and material within fibrin clots contributed to TPF signal. The increase of mucosal stiffness following triple scrape is likely due to edema and fibrosis of the lamina propria and submucosa [visible in MPM images,

Figs. 2(g) and 2(h)]. Whereas collagen concentration and microstructure contribute to E, the immune cell infiltration contributes to the TPF signal but is unlikely to contribute to increased mucosal stiffness.

The SHG depth decay coefficient depends on many signal-generating and light-scattering properties of the bulk tissue. Greater scattering from bulk tissue components or from individual collagen fibers will tend to increase the decay coefficient, because more signal is returned from the tissue surface but less from deeper layers.[34,35] The strong correlation of E with SHG depth decay coefficient from control and enzyme-treated tracheas [$R^2 = 0.77$, Fig. 5(d)] may be explained by variation within those tissues of collagen and elastin microstructure and content. Because collagen and elastin are the predominant matrix proteins of tracheal mucosa, changes in either component would be expected to influence mucosal stiffness.

Scrape-injured tracheas did not produce a correlation between SHG depth decay and E. Scrape-injured tracheas contained collagen with a finer and far more heterogeneous microstructure than fibers from the normal lamina reticularis (Fig. 3). Compared to a network of larger collagen fibers, a finer collagen network would be expected to possess a smaller SHG decay coefficient despite equal or increased collagen concentration. An inhomogeneous collagen network would possess changing collagen volume fraction with depth (unlike the relatively homogeneous normal lamina reticularis), which could introduce further variability into the correlation for scrape-injured tissues. Segmenting SHG images should correct for inhomogeneous collagen volume fraction; in fact, the correlation of E with segmented SHG signal depth decay is positive and stronger compared to unsegmented SHG signal depth decay, when comparing all tissue groups [$R^2 = 0.44$ versus $R^2 = 0.20$, Figs. 5(d) and 5(e)] although this positive correlation implies that some information on mucosal mechanics may be derived from simple multiphoton image parameters, such as SHG depth decay, some variation in bulk E remains unexplained.

One simple theory that may explain the mechanical properties of complex tissue, such as the mucosa, is composites theory, in which bulk E is related to a linear combination of constituent volume fractions weighted by the constituent Young's moduli.[42] Other tissue constituents, such as capillaries, fibrin, and nonfluorescent cells likely contribute to bulk tissue mechanics, yet remain undetected by MPM. Signal scattering by these constituents should contribute, though perhaps weakly, to the SHG decay coefficient. Fluorescent labeling of cells and matrix constituents may be necessary to completely characterize the microstructure-mechanics relationship of superficial mucosa, including the role of blood vessels [see Fig. 3(c)].

Finally, an additional source of variability in the correlations between SHG and TPF image parameters with bulk E is the size of the sampling area. The multiphoton images, which are used in the determination of area fraction and depth decay, are only 0.05 mm^2 (225×225 μm), which is roughly 4% of the area of the indentation probe (1.3 mm diam, or 1.33 mm^2). Figure 3 demonstrates the significant heterogeneity in the SHG and TPF signals over an area of 1.26 mm^2

(1.125×1.125 mm), which is approximately the area of the mechanical testing platen.

In summary, the ability of MPM to assess tissue stiffness depends on selection of appropriate image parameters that yield mechanically relevant information about tissue content and microstructure. The segmented SHG signal decay coefficient is one such parameter that relates information about tissue scattering, absorption, and collagen content—in an instrument-independent and noninvasive fashion—providing insight into bulk tissue mechanics. The TPF signal yields information about fluorescing components within a complex connective tissue that complement information derived from SHG signal. With the continued development of multiphoton and laser microscope endoscopy, a combination of SHG and TPF signal parameters may be useful to noninvasively characterize *in vivo* remodeling of collagen- and elastin-rich tissues, including tracheal mucosa, visceral pericardium, skin, and blood vessel walls.

References

1. Y. Morishima, A. Nomura, Y. Uchida, Y. Noguchi, T. Sakamoto, Y. Ishii, Y. Goto, K. Masuyama, M. J. Zhang, K. Hirano, M. Mochizuki, M. Ohtsuka, and K. Sekizawa, "Triggering the induction of myofibroblast and fibrogenesis by airway epithelial shedding," *Am. J. Respir. Cell Mol. Biol.* **24**(1), 1–11 (2001).
2. S. Zhang, H. Smartt, S. T. Holgate, and W. R. Roche, "Growth factors secreted by bronchial epithelial cells control myofibroblast proliferation: an *in vitro* co-culture model of airway remodeling in asthma," *Lab. Invest.* **79**(4), 395–405 (1999).
3. T. A. Wynn, "Cellular and molecular mechanisms of fibrosis," *J. Pathol.* **214**(2), 199–210 (2008).
4. H. G. Thompson, J. D. Mih, T. B. Krasieva, B. J. Tromberg, and S. C. George, "Epithelial-derived TGF-beta2 modulates basal and wound-healing subepithelial matrix homeostasis," *Am. J. Physiol. Lung Cell. Mol. Physiol.* **291**(6), L1277–1285 (2006).
5. N. K. Malavia, J. D. Mih, C. B. Raub, B. T. Dinh, and S. C. George, "IL-13 induces a bronchial epithelial phenotype that is profibrotic," *Resp. Res.* **9**, 27 (2008).
6. B. Hinz, "Tissue stiffness, latent TGF-beta1 activation, and mechanical signal transduction: implications for the pathogenesis and treatment of fibrosis," *Curr. Rheumatol. Rep.* **11**(2), 120–126 (2009).
7. P. J. Wipff, D. B. Rifkin, J. J. Meister, and B. Hinz, "Myofibroblast contraction activates latent TGF-beta1 from the extracellular matrix," *J. Cell Biol.* **179**(6), 1311–1323 (2007).
8. K. J. Parker, L. S. Taylor, S. Gracewski, and D. J. Rubens, "A unified view of imaging the elastic properties of tissue," *J. Acoust. Soc. Am.*

117(5), 2705–2712 (2005).

9. N. A. Goldstein, P. A. Hebda, E. C. Klein, and J. E. Dohar, "Wound management of the airway mucosa: comparison with skin in a rabbit model," *Int. J. Pediatr. Otorhinolaryngol.* **45**(3), 223–235 (1998).

10. B. G. Zani, K. Kojima, C. A. Vacanti, and E. R. Edelman, "Tissue-engineered endothelial and epithelial implants differentially and synergistically regulate airway repair," *Proc. Natl. Acad. Sci. U.S.A.* **105**(19), 7046–7051 (2008).

11. N. K. Malavia, C. B. Raub, S. B. Mahon, M. Brenner, R. A. Panettieri, Jr., and S. C. George, "Airway epithelium stimulates smooth muscle proliferation," *Am. J. Respir. Cell Mol. Biol.* **41**(3), 297–304 (2009).

12. Y. Nakagishi, Y. Morimoto, M. Fujita, Y. Ozeki, T. Maehara, and M. Kikuchi, "Rabbit model of airway stenosis induced by scraping of the tracheal mucosa," *Laryngoscope* **115**(6), 1087–1092 (2005).

13. C. B. Raub, V. Suresh, T. Krasieva, J. Lyubovitsky, J. D. Mih, A. J. Putnam, B. J. Tromberg, and S. C. George, "Noninvasive assessment of collagen gel microstructure and mechanics using multiphoton microscopy," *Biophys. J.* **92**(6), 2212–2222 (2007).

14. C. B. Raub, J. Unruh, V. Suresh, T. Krasieva, T. Lindmo, E. Gratton, B. J. Tromberg, and S. C. George, "Image correlation spectroscopy of multiphoton images correlates with collagen mechanical properties," *Biophys. J.* **94**(6), 2361–2373 (2008).

15. A. Zoumi, A. Yeh, and B. J. Tromberg, "Imaging cells and extracellular matrix *in vivo* by using second-harmonic generation and two-photon excited fluorescence," *Proc. Natl. Acad. Sci. U.S.A.* **99**(17), 11014–11019 (2002).

16. W. R. Zipfel, R. M. Williams, R. Christie, A. Y. Nikitin, B. T. Hyman, and W. W. Webb, "Live tissue intrinsic emission microscopy using multiphoton-excited native fluorescence and second harmonic generation," *Proc. Natl. Acad. Sci. U.S.A.* **100**(12), 7075–7080 (2003).

17. I. Georgakoudi, W. L. Rice, M. Hronik-Tupaj, and D. L. Kaplan, "Optical spectroscopy and imaging for the noninvasive evaluation of engineered tissues," *Tissue Eng.* **14**(4), 321–340 (2008).

18. N. D. Kirkpatrick, J. B. Hoying, S. K. Botting, J. A. Weiss, and U. Utzinger, "*In vitro* model for endogenous optical signatures of collagen," *J. Biomed. Opt.* **11**(5), 054021 (2006).

19. T. Theodossiou, G. S. Rapti, V. Hovhannisyan, E. Georgiou, K. Politopoulos, and D. Yova, "Thermally induced irreversible conformational changes in collagen probed by optical second harmonic generation and laser-induced fluorescence," *Lasers Med. Sci.* **17**(1), 34–41 (2002).

20. K. Konig, A. Ehlers, I. Riemann, S. Schenkl, R. Buckle, and M. Kaatz, "Clinical two-photon microendoscopy," *Microsc. Res. Tech.* **70**(5), 398–402 (2007).

21. K. Schenke-Layland, I. Riemann, O. Damour, U. A. Stock, and K. Konig, "Two-photon microscopes and *in vivo* multiphoton tomographs—powerful diagnostic tools for tissue engineering and drug delivery," *Adv. Drug Delivery Rev.* **58**(7), 878–896 (2006).

22. R. P. Barretto, B. Messerschmidt, and M. J. Schnitzer, "*In vivo* fluorescence imaging with high-resolution microlenses," *Nat. Methods* **6**(7), 511–512 (2009).

23. M. Brenner, K. Kreuter, D. Mukai, T. Burney, S. Guo, J. Su, S. Mahon, A. Tran, L. Tseng, J. Ju, and Z. Chen, "Detection of acute smoke-induced airway injury in a New Zealand white rabbit model using optical coherence tomography," *J. Biomed. Opt.* **12**(5), 051701 (2007).

24. S. L. Codd, R. K. Lambert, M. R. Alley, and R. J. Pack, "Tensile stiffness of ovine tracheal wall," *J. Appl. Physiol.* **76**(6), 2627–2635 (1994).

25. D. J. Tschumperlin and J. M. Drazen, "Mechanical stimuli to airway remodeling," *Am. J. Respir. Crit. Care Med.* **164**(10 Pt 2), S90–94 (2001).

26. B. R. Wiggs, C. A. Hrousis, J. M. Drazen, and R. D. Kamm, "On the mechanism of mucosal folding in normal and asthmatic airways," *J. Appl. Physiol.* **83**(6), 1814–1821 (1997).

27. A. Al-Attar, S. Mess, J. M. Thomassen, C. L. Kauffman, and S. P. Davison, "Keloid pathogenesis and treatment," *Plast. Reconstr. Surg.* **117**(1), 286–300 (2006).

28. H. P. Ehrlich, A. Desmouliere, R. F. Diegelmann, I. K. Cohen, C. C. Compton, W. L. Garner, Y. Kapanci, and G. Gabbiani, "Morphological and immunochemical differences between keloid and hypertrophic scar," *Am. J. Pathol.* **145**(1), 105–113 (1994).

29. B. C. Willis, J. M. Liebler, K. Luby-Phelps, A. G. Nicholson, E. D. Crandall, R. M. du Bois, and Z. Borok, "Induction of epithelial-mesenchymal transition in alveolar epithelial cells by transforming growth factor-beta1: potential role in idiopathic pulmonary fibrosis," *Am. J. Pathol.* **166**(5), 1321–1332 (2005).

30. B. C. Willis and Z. Borok, "TGF-beta-induced EMT: mechanisms and implications for fibrotic lung disease," *Cur. Osteoporosis Rep.* **293**(3), L525–534 (2007).

31. J. C. Tse and R. Kalluri, "Mechanisms of metastasis: epithelial-to-mesenchymal transition and contribution of tumor microenvironment," *J. Cell. Biochem.* **101**(4), 816–829 (2007).

32. A. Agarwal, M. L. Coleno, V. P. Wallace, W. Y. Wu, C. H. Sun, B. J. Tromberg, and S. C. George, "Two-photon laser scanning microscopy of epithelial cell-modulated collagen density in engineered human lung tissue," *Tissue Eng.* **7**(2), 191–202 (2001).

33. A. M. Pena, A. Fabre, D. Debarre, J. Marchal-Somme, B. Crestani, J. L. Martin, E. Beaurepaire, and M. C. Schanne-Klein, "Three-dimensional investigation and scoring of extracellular matrix remodeling during lung fibrosis using multiphoton microscopy," *Microsc. Res. Tech.* **70**(2), 162–170 (2007).

34. S. Zhuo, J. Chen, X. Jiang, S. Xie, R. Chen, N. Cao, Q. Zou, and S. Xiong, "The layered-resolved microstructure and spectroscopy of mouse oral mucosa using multiphoton microscopy," *Phys. Med. Biol.* **52**(16), 4967–4980 (2007).

35. A. K. Dunn, V. P. Wallace, M. Coleno, M. W. Berns, and B. J. Tromberg, "Influence of optical properties on two-photon fluorescence imaging in turbid samples," *Appl. Opt.* **39**(7), 1194–1201 (2000).

36. M. Balu, T. Baldacchini, J. Carter, T. B. Krasieva, R. Zadoyan, and B. J. Tromberg, "Effect of excitation wavelength on penetration depth in nonlinear optical microscopy of turbid media," *J. Biomed. Opt.* **14**(1), 010508 (2009).

37. R. Samatham, S. L. Jacques, and P. Campagnola, "Optical properties of mutant versus wild-type mouse skin measured by reflectance-mode confocal scanning laser microscopy (rCSLM)," *J. Biomed. Opt.* **13**(4), 041309 (2008).

38. G. Yao and L. V. Wang, "Monte Carlo simulation of an optical coherence tomography signal in homogeneous turbid media," *Phys. Med. Biol.* **44**(9), 2307–2320 (1999).

39. E. Brown, T. McKee, E. diTomaso, A. Pluen, B. Seed, Y. Boucher, and R. K. Jain, "Dynamic imaging of collagen and its modulation in tumors *in vivo* using second-harmonic generation," *Nat. Med.* **9**(6), 796–800 (2003).

40. G. M. Turino, R. V. Lourenco, and G. H. McCracken, "Role of connective tissues in large pulmonary airways," *J. Appl. Physiol.* **25**(6), 645–653 (1968).

41. P. Seethanathan, B. Radhakrishnamurthy, E. R. Dalferes, Jr., and G. S. Berenson, "The composition of connective tissue macromolecules from bovine respiratory system," *Respir. Physiol.* **24**(3), 347–354 (1975).

42. M. E. Nimni, Ed., *Collagen*, CRC Press, Boca Raton (1988).